Optics Letters

# Frequency-multiplying microwave photonic phase shifter for independent multichannel phase shifting

YAMEI ZHANG AND SHILONG PAN*

*Key Laboratory of Radar Imaging and Microwave Photonics, Ministry of Education, Nanjing University of Aeronautics and Astronautics, Nanjing 210016, China*
**Corresponding author: pans@ieee.org*

*Received 23 December 2015; accepted 20 January 2016; posted 25 January 2016 (Doc. ID 256289); published 15 March 2016*

**A frequency-multiplying microwave photonic phase shifter with independent multichannel phase shifting capability is proposed and demonstrated using an integrated polarization division multiplexing dual-parallel Mach–Zehnder modulator (PDM-DPMZM) and a polarizer. By building a proper power distribution network to drive the PDM-DPMZM, two sidebands along two orthogonal polarization directions are generated with a spacing of two or four times the frequency of the driving signal. Leading the signal to a polarizer and a photodetector, a frequency-doubled or frequency-quadrupled signal with its phase adjusted by the polarization direction of the polarizer is achieved. The magnitude of the signal remains almost unchanged when the phase is adjusted. The proposed approach features compact configuration, scalable independent phase-shift channels and wide bandwidth, which can find applications in beam forming and analog signal processing for millimeter-wave or terahertz applications.** 

***OCIS codes:*** (050.5080) Phase shift; (060.5625) Radio frequency photonics; (130.4110) Modulators.

http://dx.doi.org/10.1364/OL.41.001261

Microwave phase shifter is a fundamental component for RF beam forming, phase locking and analog signal processing, including tunable filtering, phase coding, differentiating, signal synchronization, etc. [1–3]. With the fast development of millimeter-wave and terahertz technologies, a high-frequency phase shifter [4,5] is urgently desired, since preprocessing of the large-bandwidth millimeter-wave or terahertz signal in the analog domain before digitizing would be more practical than the full digital solution due to the lack of a large bandwidth analog-to-digital converter. However, because of the well-known electronic bottleneck, direct implementation of the microwave phase shifter in the electronic domain would suffer from limited operation bandwidth, slow tuning speed, and frequency-varied phase shifting. In addition, for most phase shifter-based applications, simultaneous multichannel phase shifting is always required, which leads to serious electromagnetic interference. To solve these problems, photonic microwave phase shifters are attractive, thanks to large operation bandwidth, good frequency tunability, low transmission loss, and electromagnetic interference immunity enabled by photonic technologies [6–11]. But the maximal operational frequency of a photonic microwave phase shifter is restricted by the bandwidths of the electro-optic modulators, typically less than 50 GHz. To break through this boundary, a feasible way is to implement simultaneous frequency multiplying and phase shifting in the optical domain. However, both technologies need to manipulate polarization, phase and/or amplitude of the microwave-modulated optical signals at the same time, which would disturb each other, making the simultaneous implementation of photonic frequency multiplying and phase shifting very difficult. Previously, only very few approaches could perform the frequency-multiplying phase shifter [12–14]. In [12], a frequency-quadrupling microwave phase shifter is realized, based on orthogonally polarized carrier-suppressed double-sideband (CS-DSB) modulation and polarization modulation. An optical notch filter and a phase-shifted fiber Bragg grating (PS-FBG) with two passbands, respectively, in two orthogonal polarization directions are employed to achieve the orthogonally polarized CS-DSB modulation, and a polarization modulator (PolM) is used to introduce complementary phase shifts to the two sidebands, making the phase shifter only effective at several discrete frequencies. To implement a frequency-multiplying phase shifter with large frequency tunability, in [13,14] a programmable optical filter based on liquid crystal on silicon is employed. Because the programmable optical filter can control the amplitude and phase of any optical spectral component, the two optical sidebands, i.e., ±1st-order sidebands [13] or ±2nd-order sidebands [14] can be selected, and a phase shift is introduced to one of the two sidebands simultaneously. However, the programmable optical filter is usually realized based on free-space optics, which is bulky and expensive. In addition, it is hard for this kind of method to implement large-array multichannel phase shifting, since the output ports of the programmable optical filter are typically limited to four.

In this Letter, a frequency-multiplying full-range tunable microwave photonic phase shifter with independent multichannel phase shifting capability is proposed and experimentally demonstrated.

Figure 1 shows the schematic diagram of the proposed multichannel microwave photonic phase shifter. Each channel consists of a shared laser diode (LD), a shared integrated polarization division multiplexing dual-parallel Mach–Zehnder modulator (PDM-DPMZM), two polarization controllers (PCs), a polarizer, and a photodetector (PD). An optical carrier generated by the LD is sent to the PDM-DPMZM. A PC ($PC_1$) is inserted to align the polarization direction of the optical carrier to have an angle of 45 deg to one principal axis of the PDM-DPMZM. The equivalent schematic of the PDM-DPMZM is shown in the dotted box in Fig. 1, which consists of two parallel DPMZMs connected by a polarization beam splitter (PBS) and a polarization beam combiner (PBC). The device has four RF input ports and six DC biases, so it has enough degrees of freedom to manipulate the optical signal. Suppose the expression of the optical carrier is $\exp(j\omega_c t)$ and those of the RF signals introduced to the four RF ports are $V_{\mathrm{RF}}\cos(\omega_{\mathrm{RF}}t+\phi_1)$, $V_{\mathrm{RF}}\cos(\omega_{\mathrm{RF}}t+\phi_2)$, $V_{\mathrm{RF}}\cos(\omega_{\mathrm{RF}}t+\phi_3)$, and $V_{\mathrm{RF}}\cos(\omega_{\mathrm{RF}}t+\phi_4)$, respectively, where $\omega_c$ is the angular frequency of the optical carrier, $\omega_{\mathrm{RF}}$, $\phi_i(I=1,2,3,4)$, and $V_{\mathrm{RF}}$ are the angular frequency, phases, and magnitude (assumed to be the same) of the four RF signals, the modulated signal after the PDM-DPMZM can be written as

$$\begin{cases} E_x = \cos(\omega_c t)[\cos(\beta\cos(\omega_{\mathrm{RF}}t+\phi_1)+\theta_1/2)\exp(j\theta_3) \\ +\cos(\beta\cos(\omega_{\mathrm{RF}}t+\phi_2)+\theta_2/2)] \\ E_y = \cos(\omega_c t)[\cos(\beta\cos(\omega_{\mathrm{RF}}t+\phi_3)+\theta_4/2)\exp(j\theta_6) \\ +\cos(\beta\cos(\omega_{\mathrm{RF}}t+\phi_4)+\theta_5/2)], \end{cases} \tag{1}$$

where $x$ and $y$ represent the two principal axes of the PDM-DPMZM, $\beta=\pi V_{\mathrm{RF}}/V\pi$ is the modulation index, $V\pi$ is the half-wave voltage, $\theta_m=\pi V_{\mathrm{DC}m}/V\pi(m=1,2,3,4,5,6)$ are the phase differences introduced by the DC biases of the sub-MZMs, and $V_{\mathrm{DC}m}$ are the voltages of the DC biases.

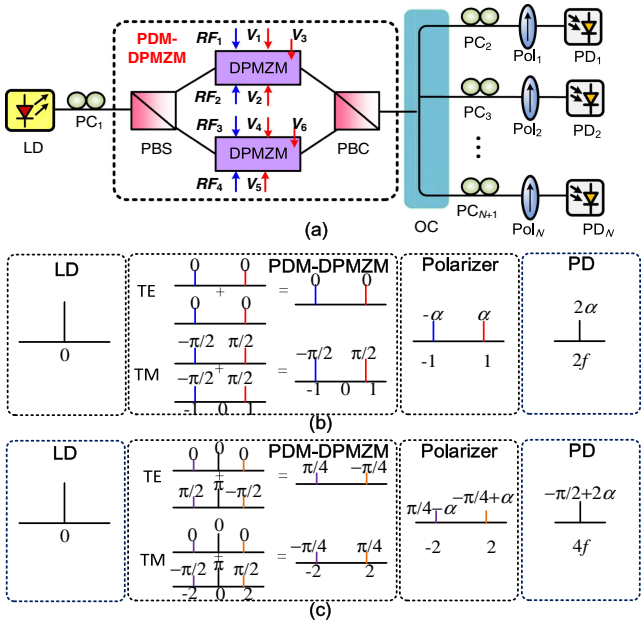


**Fig. 1.** (a) Schematic of the proposed frequency-multiplying microwave photonic phase shifter with independent multichannel phase shifting capability, and schematics of the optical spectra after different devices for (b) frequency-doubling and (c) frequency-quadrupling operations. LD: laser diode; PC: polarization controller; OC: optical coupler; PDM-DPMZM: polarization division multiplexing dual-parallel Mach–Zehnder modulator; PBS: polarization beam splitter; PBC: polarization beam combiner; PD: photodetector.

To implement the frequency-doubling phase shifter, the four sub-MZMs are biased at the minimum transmission points by controlling the DC biases to let $\theta_1=\theta_2=\theta_4=\theta_5=\pi$ and $\theta_3=\theta_6=0$. Expanding Eq. (1) with Bessel functions and rewriting it with the exponential form, the signal becomes

$$\begin{cases} E_x = \exp(j\omega_c t)[-J_{-1}(\beta)\exp(-j(\omega_{\mathrm{RF}}t+\phi_1)) \\ -J_1(\beta)\exp(j(\omega_{\mathrm{RF}}t+\phi_1))-J_{-1}(\beta)\exp(-j(\omega_{\mathrm{RF}}t+\phi_2)) \\ -J_1(\beta)\exp(j(\omega_{\mathrm{RF}}t+\phi_2))] \\ E_y = \exp(j\omega_c t)[-J_{-1}(\beta)\exp(-j(\omega_{\mathrm{RF}}t+\phi_3)) \\ -J_1(\beta)\exp(j(\omega_{\mathrm{RF}}t+\phi_3))-J_{-1}(\beta)\exp(-j(\omega_{\mathrm{RF}}t+\phi_4)) \\ -J_1(\beta)\exp(j(\omega_{\mathrm{RF}}t+\phi_4))], \end{cases} \tag{2}$$

where $J_m$ is the Bessel function of the first kind of order $m$. In writing Eq. (2), small-signal modulation is assumed so that the higher-order ($\geq 2$) sidebands are ignored. Adjusting the phases of the RF signals to let $\phi_1=\phi_2=0$ and $\phi_3=\phi_4=\pi/2$, Eq. (2) can be simplified to

$$\begin{cases} E_x = \exp(j\omega_c t)[-2J_{-1}(\beta)\ \exp(-j(\omega_{\mathrm{RF}}t)) \\ -2J_1(\beta)\ \exp(j(\omega_{\mathrm{RF}}t))] \\ E_y = \exp(j\omega_c t)[-2J_{-1}(\beta)\ \exp(-j(\omega_{\mathrm{RF}}t+\pi/2)) \\ -2J_1(\beta)\ \exp(j(\omega_{\mathrm{RF}}t+\pi/2))]. \end{cases} \tag{3}$$

As can be seen, two CS-DSB-modulated signals are generated along the two orthogonal polarization directions. In addition, the phase difference between the two −1st-order sidebands in $E_x$ and $E_y$ is $\pi/2$, while that of the +1st-order sidebands is $-\pi/2$. The two orthogonally polarized CS-DSB-modulated signals are then combined by the PBC and sent to the polarizer, which has an angle of $\alpha$ to one principal axis of the PDM-DPMZM. We obtain that

$$\begin{aligned} E_{\mathrm{out}}(t) &= \cos\alpha E_x + \sin\alpha E_y \\ &= \exp(j\omega_c t)[-2J_{-1}(\beta)\ \exp(-j(\omega_{\mathrm{RF}}t+\alpha)) \\ &\quad -2J_1(\beta)\ \exp(j(\omega_{\mathrm{RF}}t+\alpha))]. \end{aligned} \tag{4}$$

Leading the signal in Eq. (4) to the PD for square-law detection, we can obtain an electrical current given by

$$I_{\mathrm{AC}}(t)\propto J_{-1}(\beta)J_1(\beta)\cos(2\omega_{\mathrm{RF}}t+2\alpha). \tag{5}$$

As can be seen from Eq. (5), the generated signal has an angular frequency of $2\omega_{\mathrm{RF}}$ and a phase term of $2\alpha$. By simply controlling the angle $\alpha$ between the polarization direction of the polarizer and one principal axis of the PDM-DPMZM, the phase of the generated signal can be continuously tuned. As a result, a frequency-doubling phase shifter is realized. Figure 1(b) depicts the schematics of the optical spectra under this condition.

If the sub-MZMs are biased at the maximum transmission points by controlling the DC biases of the PDM-DPMZM to let $\theta_1=\theta_2=\theta_4=\theta_5=0$ and $\theta_3=\theta_6=\pi$, the output of the PDM-DPMZM becomes

$$\begin{cases} E_x = \exp(j\omega_c t)[J_{-2}(\beta)\exp(-j2(\omega_{\mathrm{RF}}t+\phi_1)) \\ +J_2(\beta)\ \exp(j2(\omega_{\mathrm{RF}}t+\phi_1))-J_{-2}(\beta)\ \exp(-j2(\omega_{\mathrm{RF}}t+\phi_2)) \\ -J_2(\beta)\ \exp(j2(\omega_{\mathrm{RF}}t+\phi_2))] \\ E_y = \exp(j\omega_c t)[J_{-2}(\beta)\ \exp(-j2(\omega_{\mathrm{RF}}t+\phi_3)) \\ +J_2(\beta)\ \exp(j2(\omega_{\mathrm{RF}}t+\phi_3))-J_{-2}(\beta)\ \exp(-j2(\omega_{\mathrm{RF}}t+\phi_4)) \\ +J_2(\beta)\ \exp(j2(\omega_{\mathrm{RF}}t+\phi_4))]. \end{cases} \tag{6}$$

Then adjusting the phases of the input RF signals to let $\phi_1 = 0, \phi_2 = \pi/4, \phi_3 = 0$, and $\phi_4 = -\pi/4$, we obtain

$$\begin{cases} E_x = \exp(j\omega_c t)[-\sqrt{2}J_{-2}(\beta)\ \exp(-j2\omega_{RF}t + j\pi/4) \\ -\sqrt{2}J_2(\beta)\ \exp(j2\omega_{RF}t - j\pi/4)] \\ E_y = \exp(j\omega_c t)[-\sqrt{2}J_{-2}(\beta)\ \exp(-j2\omega_{RF}t - j\pi/4) \\ -\sqrt{2}J_2(\beta)\ \exp(j2\omega_{RF}t + j\pi/4)]. \end{cases} \quad (7)$$

As can be seen, CS-DSB-modulated signals with only ±2nd-order sidebands are generated along both polarization directions. The phase difference between the two −2nd-order sidebands in $E_x$ and $E_y$ is $\pi/2$, while that of the +2nd-order sidebands is $-\pi/2$. When the two signals are combined by the PBC, transmitted through the polarizer, and beat at the PD, we can achieve an output current with the form of

$$I_{AC}(t) \propto J_{-2}(\beta)J_2(\beta)\cos\left(4\omega_{RF}t - \frac{\pi}{2} + 2\alpha\right). \quad (8)$$

As can be seen, a frequency-quadrupling phase shifter is implemented as the generated current has an angular frequency of $4\omega_{RF}$ and a phase of $2\alpha$. The schematics of the optical spectra after different devices for frequency-quadrupling operation are shown in Fig. 1(c).

It should be noted that the PC placed before the polarizer, which is used to adjust $\alpha$, can be replaced by an electronically controlled PC or a PolM, so the proposed microwave photonic phase shifter can be tuned at a very fast speed (as fast as 50 Gb/s [15]). In addition, due to the phase shifting is independently controlled by the PC placed before the polarizer, the output of the PDM-DPMZM can be split into $N$ paths, and in each path, a PC, a polarizer, and a PD is inserted to implement phase shifting independently. Thereby, a scalable multichannel frequency-multiplying phase shifter can be realized with compact configuration.

To demonstrate the feasibility of the proposed frequency-multiplying phase shifter, a proof-of-concept experiment is carried out based on the configuration of Fig. 1. A light wave from a tunable laser source (Agilent N7714A) with a wavelength of 1552.52 nm and a power of 13 dBm is sent to a PDM-DPMZM (Fujitsu FTM7977HQA). The 3 dB bandwidth and half-wave voltage of the PDM-DPMZM are 23 GHz and 3.5 V, respectively. The modulator is driven by four RF signals obtained by splitting one RF signal from a signal generator (Agilent 8257D) with electrical power dividers (2–18 GHz), a 90 deg hybrid (1.7–36 GHz), and/or a 180 deg hybrid (2-18 GHz). By carefully adjusting the phases of the driving signal and the DC biases of the modulator, CS-DSB signals with ±1st-order sidebands or ±2nd-order sidebands are generated. A PC and a PBS are inserted to serve as a polarizer, and a PD with a bandwidth of 40 GHz and a responsivity of 0.65A/W is used to perform optical-to-electrical conversion. An erbium-doped fiber amplifier (EDFA) is employed to compensate the insertion loss. The optical spectra are measured by an optical spectrum analyzer (OSA, AQ6370C), and the waveforms of the generated signals are observed by a digital sampling oscilloscope (Agilent 86100C).

For the frequency-doubling phase shifter, the PDM-DPMZM is driven by RF signals with phases of $\phi_1 = \phi_2 = 0, \phi_3 = \phi_4 = \pi/2$. To achieve such RF signals, a 7.5-GHz signal from the RF source is split into two parts using a broadband 90 deg hybrid, and further split into four portions using two power dividers, as shown in Fig. 2(a). The DC biases are adjusted to let $\theta_1 = \theta_2 = \theta_4 = \theta_5 = \pi$ and $\theta_3 = \theta_6 = 0$. Figure 3 shows the spectrum of the CS-DSB-modulated signal.

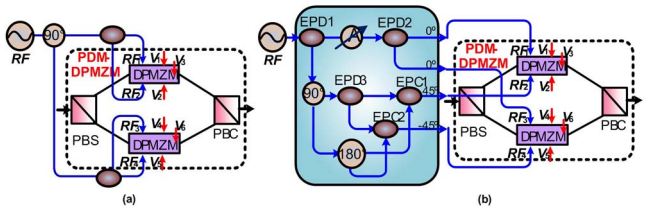


**Fig. 2.** Experimental setup of the PDM-DPMZM for (a) frequency-doubling and (b) frequency-quadrupling phase shifters. EPD: electrical power divider; EPC: electrical power combiner.

As can be seen, two ±1st-order sidebands with a spacing of 15 GHz are generated, and the optical carrier is suppressed to be 24 dB lower than the sidebands.

Figure 4 shows the waveforms of the generated frequency-doubled 15 GHz signal with its phase tuned from −180 deg to 180 deg. As can be seen, full-range phase tunability is confirmed, and the amplitude of the generated signal during phase shifting remains almost unchanged. The very small amplitude variation is mainly introduced by the uneven insertion loss of the PC. To confirm the frequency agility of the proposed system, a RF signal with a frequency of 13 GHz is also applied to the system. The waveforms of the generated signals with different phase shifts are shown in Fig. 5. By simply adjusting the angle between the polarization direction of the polarizer and one principal axis of the PDM-DPMZM, the phase can be continuously tuned while the amplitude remains unchanged.

To realize the frequency-quadrupling phase shifter, the phases of the input RF signals and the DC biases are adjusted to let $\phi_1 = 0, \phi_2 = \pi/4, \phi_3 = 0$, $\phi_4 = -\pi/4, \theta_1 = \theta_2 = \theta_4 = \theta_5 = 0$, and $\theta_3 = \theta_6 = \pi$. In order to obtain broadband 0, $\pi/4$, and $-\pi/4$ phase shifts, another power distribution

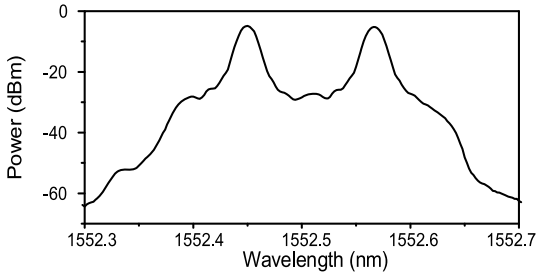


**Fig. 3.** Optical spectrum of the CS-DSB-modulated signal at the output of the PDM-DPMZM for frequency-doubling phase shifter.

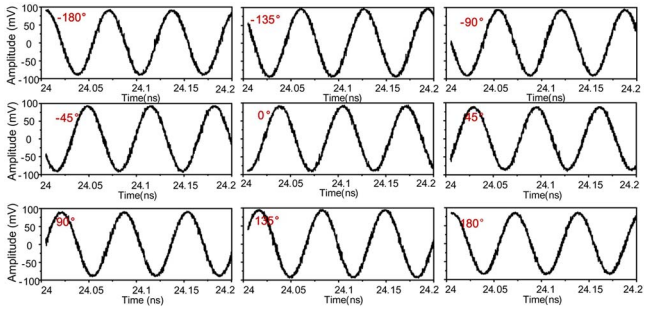


**Fig. 4.** Waveforms of the generated frequency-doubled 15 GHz signals with the phase tuned from −180 deg to 180 deg.

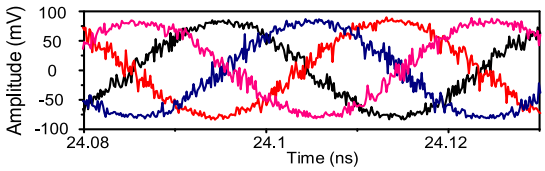


**Fig. 5.** Waveforms of the generated frequency-doubled 26 GHz signals with different phase shifts.

network is designed, which is shown in Fig. 2(b). The RF signal from the signal generator is first split into two paths with an electrical power divider (EPD1). The signal in the upper path is further split into two parts with another electrical power divider (EPD2) to achieve two RF signals with a phase of 0, while that in the lower path is used to generate two RF signals with phases of $-\pi/4$ and $\pi/4$, respectively, via one 90 deg hybrid, one 180 deg hybrid, one power divider, and two power combiners. Due to the bandwidth of the 90 deg hybrid, the 180 deg hybrid, the power divider, and the power combiner can be very large; the $\pm 45$ deg phase shifts can be almost frequency-independent in the frequency range of interest. Figure 6 shows the optical spectrum of the CS-DSB-modulated signal generated at the output of the PDM-DPMZM when an electrical driving signal with a frequency of 8 GHz is applied. As can be seen, two ±2nd-order sidebands are obtained, and the optical carrier is about 27 dB lower than the sidebands. Figure 7 shows the waveforms of the generated signal, where different curves represent waveforms with different phase shifts. During the phase shifting, the amplitude of the generated signal remains unchanged. The frequency of the generated signal is calculated to be 32 GHz. When a 10 GHz RF signal driving signal is applied, 40 GHz signal with full-range phase tunability is also generated, showing that the proposed system has a good frequency agility. The noise among the signals is mainly due to

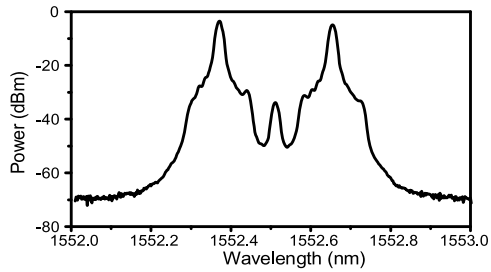


**Fig. 6.** Optical spectrum of the CS-DSB-modulated signal at the output of the PDM-DPMZM for frequency-quadrupling phase shifter.

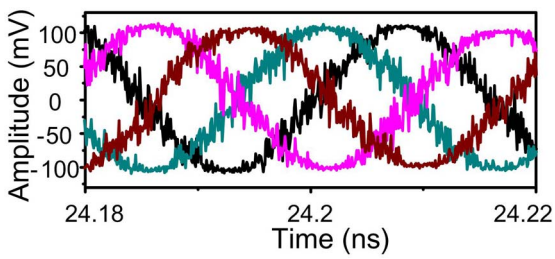


**Fig. 7.** Waveforms of the generated frequency-quadrupled 32 GHz signals with different phases.

the small modulation index of the PDM-DPMZM and the amplified spontaneous emission of the EDFA. If the modulation index is increased, the signal-to-noise ratio can be increased.

It should be noted that the proposed system could have a large operation bandwidth due to the frequency-multiplying operation. Given that the operational frequency range of the 180 deg hybrid used in the experiment is 2–18 GHz, the proposed phase shifter can be operated in a frequency range from 4 to 72 GHz. If electrical devices with larger operation bandwidth are used, phase shifters operated in the higher-frequency regime can be realized.

In conclusion, a novel microwave photonic phase shifter featuring frequency-multiplying and independent multichannel phase-shifting capability was proposed and demonstrated based on a PDM-DPMZM. In a proof-of-concept experiment, a 26 GHz frequency-doubled signal and a 40 GHz frequency-quadrupled signal were generated, with their phases tuned from −180 deg to 180 deg. The magnitude of the signal kept almost unchanged when the phase was adjusted. The approach can be used for millimeter-wave or terahertz signal processing and beam forming [16–18].

**Funding.** National Basic Research Program of China (2012CB315705); National Natural Science Foundation of China (NSFC) (61422108, 61527820); Aviation Science Foundation of China (2013ZC52050); Outstanding Doctoral Dissertation in NUAA (BCXJ15-02); Jiangsu Innovation Program for Graduate Education (KYLX15_0280); Fundamental Research Funds for the Central Universities.

## REFERENCES

1. K. Ghorbani, A. Mitchell, R. B. Waterhouse, and M. W. Austin, IEEE Trans. Microwave Theory Tech. **47**, 645 (1999).
2. J. Capmany, B. Ortega, and D. Pastor, J. Lightwave Technol. **24**, 201 (2006).
3. J. P. Yao, J. Lightwave Technol. **27**, 314 (2009).
4. H.-T. Chen, W. J. Padilla, M. J. Cich, A. K. Azad, R. D. Averitt, and A. J. Taylor, Nat. Photonics **3**, 148 (2009).
5. C. F. Hsieh, R. P. Pan, T. T. Tang, H. L. Chen, and C. L. Pan, Opt. Lett. **31**, 1112 (2006).
6. J. Sancho, J. Lloret, I. Gasulla, S. Sales, and J. Capmany, Opt. Express **19**, 17421 (2011).
7. P. Qu, C. Liu, W. Dong, W. Chen, F. Li, H. Li, Z. Gong, S. Ruan, X. Zhang, and J. Zhou, Appl. Opt. **50**, 2523 (2011).
8. M. Burla, L. R. Cortés, M. Li, X. Wang, L. Chrostowski, and J. Azaña, Opt. Lett. **39**, 6181 (2014).
9. M. Pagani, D. Marpaung, D.-Y. Choi, S. J. Madden, B. L. Davies, and B. J. Eggleton, Opt. Express **22**, 28810 (2014).
10. S. Pan and Y. Zhang, Opt. Lett. **37**, 4483 (2012).
11. E. Chan, W. Zhang, and R. Minasian, J. Lightwave Technol. **30**, 3672 (2012).
12. W. F. Zhang and J. P. Yao, IEEE Photon. J. **4**, 889 (2012).
13. Z. H. Feng, S. N. Fu, T. Ming, and D. M. Liu, IEEE Photon. J. **6**, 5500108 (2014).
14. H. Z. Li, T. Y. Huang, C. J. Ke, S. N. Fu, P. P. Shum, and D. M. Liu, IEEE Photon. Technol. Lett. **26**, 220 (2014).
15. J. D. Bull, H. Kato, A. R. Reid, M. Fairburn, B. P. Tsou, D. R. Seniuk, P. H. Lu, and N. A. Jaeger, in *Conference on Lasers and Electro-Optics/Quantum Electronics and Laser Science Conference (QELS) and Photonic Applications, Systems Technologies* (2005), paper JTuC54.
16. Y. M. Zhang and S. L. Pan, Opt. Lett. **38**, 766 (2013).
17. Y. M. Zhang and S. L. Pan, Opt. Lett. **38**, 802 (2013).
18. Y. M. Zhang, H. Wu, D. Zhu, and S. L. Pan, Opt. Express **22**, 3761 (2014).